Proceedings of the ASME 2013 International Design Engineering Technical Conferences and Computers and Information in Engineering Conference
IDETC/CIE 2013
August 4-7, 2013, Portland, Oregon, USA

DETC2013-12798

CRITICAL TIMESCALES FOR BURROWING IN UNDERSEA SUBSTRATES VIA LOCALIZED FLUIDIZATION, DEMONSTRATED BY ROBOCLAM: A ROBOT INSPIRED BY ATLANTIC RAZOR CLAMS

Amos G. Winter, V*
Dept. of Mechanical Engineering
Massachusetts Institute of Technology
Cambridge, Massachusetts 02139
Email: awinter@mit.edu

Robin L. H. Deits
Dept. of Electrical Engineering and Computer Science
Massachusetts Institute of Technology
Cambridge, Massachusetts 02139
Email: rdeits@mit.edu

Daniel S. Dorsch
Dept. of Mechanical Engineering
Massachusetts Institute of Technology
Cambridge, Massachusetts 02139
Email: dorsch@mit.edu

ABSTRACT

The Atlantic razor clam (Ensis directus) burrows into underwater soil by using motions of its shell to locally fluidize the surrounding substrate. The energy associated with movement through fluidized soil – characterized by a depth-independent density and viscosity – scales linearly with depth. In contrast, moving through static soil requires energy that scales with depth squared. For E. directus, this translates to a 10X reduction in the energy required to reach observed burrow depths. For engineers, localized fluidization offers a mechanically simple and purely kinematic method to dramatically reduce burrowing energy. This concept is demonstrated with RoboClam, an E. directus-inspired robot. Using a genetic algorithm to generate digging kinematics, RoboClam has achieved localized fluidization and burrowing performance comparable to that of the animal, with a linear energy-depth relationship. In this paper, we present the critical timescales and associated kinematics necessary for achieving localized fluidization, which are calculated from soil parameters and validated via RoboClam and E. directus testing.

INTRODUCTION

Burrowing in soil presents challenges to nature and engineering alike. Many animals have developed unique locomotion schemes to move through particulate substrates [1]. The sandfish lizard (*S. scincus*) undulates in the manner of a fish in order to effectively swim through sand [2]. Clam worms (*N. virens*) have been observed to use crack propagation to burrow in gelatin, a material with similar properties to elastic muds [3]. Smaller organisms, like nematodes (*C. elegans*), have been observed to move efficiently via reciprocating motion in saturated granular media [4, 5].

Contrary to a generalized Newtonian fluid, in which viscosity and density do not change with depth, particles within a static granular material experience contact stresses, and thus frictional forces, that scale with the surrounding pressure, resulting in shear strength that increases linearly with depth [6]. This means that submerging devices such as anchors and piles can be costly, as insertion forces $F(z)$, increase linearly with depth z [7], resulting in an insertion energy, $E = \int F(z)\,dz$, that scales with depth squared.

Ensis directus, the Atlantic razor clam, can produce approximately 10N of force to pull its valves into soil [8]. Using measurements from a blunt body the size and shape of *E. directus*, we determined that this level of force enables the clam to submerge approximately 1–2cm into a packed bed. But in reality, razor clams dig to 70cm [9][1], indicating that the animal must manipulate surrounding soil to reduce burrowing drag and the energy

*Address all correspondence to this author.

[1] [9] relates the stout razor clam (*T. plebeius*); burrowing depths on this order have also been observed by the authors while collecting *E. directus* in Gloucester, MA.

required for submersion.

E. directus burrows by using a series of valve and foot motions to draw itself into the substrate (Figs. 1A–E). An upper bound of the mechanical energy associated with digging can be estimated by adapting results from Trueman [8] and summing the energies and kinematics associated with each stage during one burrow cycle: valve uplift (0.05J, -0.5cm), valve contraction (0.07J, 0cm), and valve penetration (0.20J, 2.0cm), combine for a total of 0.21J/cm (with positive displacements relating to downwards progress into the soil). Re-expansion of the valves is accomplished through elastic rebound of the hinge ligament, and thus requires no additional energy input by the animal. Comparing this performance to the energy required to push an *E. directus*-shaped blunt body into the animal's habitat substrate using steady downward force (Fig. 1F), the animal is able to reduce its required burrowing energy by an order of magnitude, even though there is an energetic cost associated with pushing up and contracting its valves – motions that do not directly contribute to downward progress. To put this performance in an engineering perspective, *E. directus* can travel over a half kilometer through soil on the energy in a AA battery [10]!

The uplift and contraction motions of *E. directus'* valves locally fail and fluidize the soil surrounding the animal's body, reducing drag forces on the clam to within its strength capabilities [11]. In an idealized fluidized medium, the drag force on a body does not depend on depth. As a result, burrowing energy scales linearly with depth for *E. directus*, rather than depth squared for the blunt body (Fig. 1F). Due to this exponential decrease in burrowing energy compared to moving through static soil, localized fluidization offers potential value to many industrial applications such as anchoring, oil recovery, mine neutralization, and cable installation. For example, an *E. directus*-based anchor is predicted to provide more than ten times the anchoring force per insertion energy as existing technologies [12].

The RoboClam robot was developed as a test bench to explore the parametric relationships behind localized fluidization burrowing and how it can be adapted into engineering applications. This paper presents experimental findings that show RoboClam is able to achieve localized fluidization while burrowing. Three critical timescales related to the robot's kinematics and the substrate's properties are theoretically derived. These parametric relationships agree with experimental data and form the basis of design rules for localized fluidization burrowing machines.

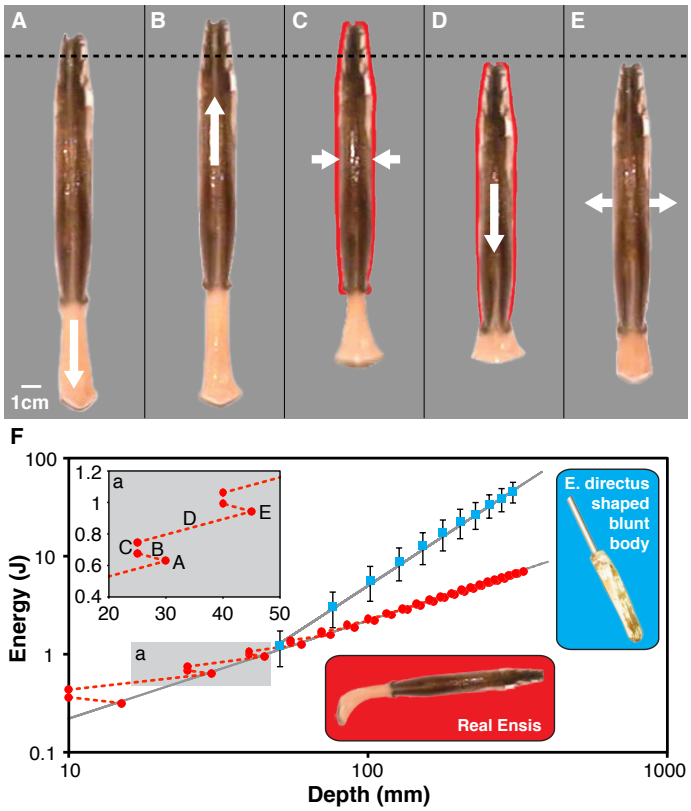

FIGURE 1. *E. DIRECTUS* DIGGING CYCLE KINEMATICS AND ENERGETICS. Dotted line in A)-E) denotes a depth datum. White arrows indicate valve movements. Red silhouette denotes valve geometry in expanded state, before contraction. A) *E. directus* at initiation of digging cycle and extension of foot. B) Valve uplift. C) Valve contraction, which pushes blood into the foot, expanding it to serve as a terminal anchor. D) Retraction of foot and downwards pull on the valves. E) Valve expansion, reset for next digging cycle. F) Energetic comparison showing that *E. directus* requires an order of magnitude less energy to submerge to burrow depth than a blunt body of the same size and shape pushed into static soil. Because *E. directus* moves through locally fluidized soil, its burrowing energy scales linearly with depth, rather than depth squared. Inset a) shows how *E. directus'* valve kinematics correlate to energetics in the burrowing cycle. Although there is an energetic cost to fluidizing the soil, doing so provides significant overall energetic savings compared to moving through static soil. *E. directus* data adapted from [8]. Blunt body data collected from 15 penetration tests in real *E. directus* habitat off the coast of Gloucester, MA

MATERIALS AND METHODS

RoboClam replicates *E. directus* digging kinematics and measures the energy expended while it burrows [13]. The robot consists of a base with two pneumatic pistons (Fig. 2A) that actuate an *E. directus*-like end effector in the same motions shown in Figs. 1A–E. The results presented in this work correspond to the end effector moving in and out only while burrowing (Fig. 2B, corresponding to *E. directus* in Figs. 1C,E), as these motions contribute to the majority of fluidization around the animal [11] and the robot was able to successfully burrow without using up/down motions (corresponding to Figs. 1B,D). The end effector is composed of a sliding wedge linkage that forces two

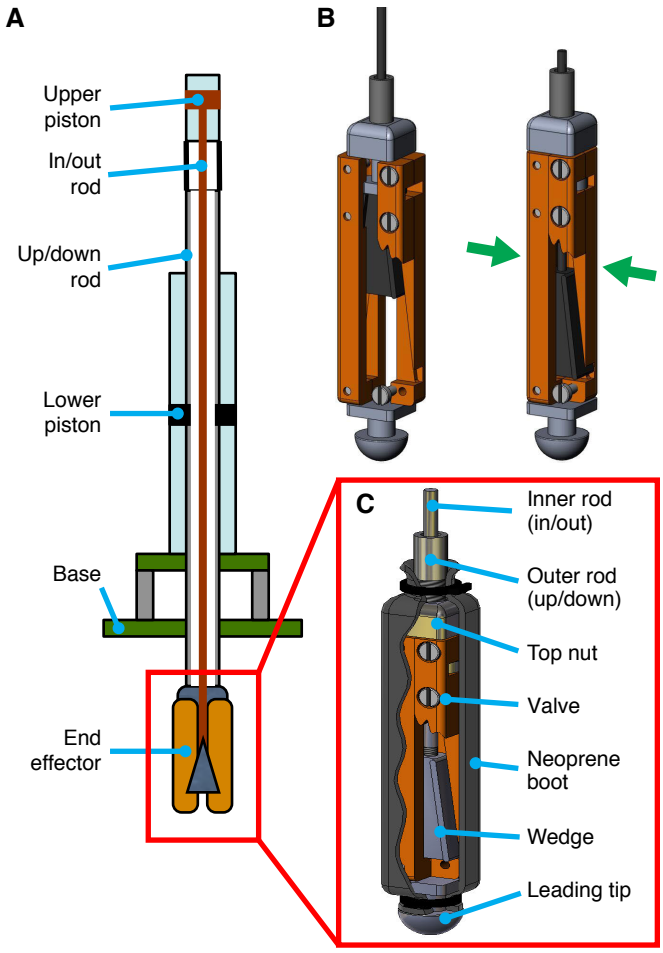

FIGURE 2. ROBOCLAM BIOMIMETIC BURROWING ROBOT. A) Schematic of the actuation architecture of the robot. The upper piston moves the end effector in and out; the lower piston moves it up and down. B) Contraction of the end effector (motion shown with arrows) with cutaway of the sliding wedge linkage. C) Schematic of the entire end effector package. The neoprene boot prevents soil particles from jamming the mechanism. The inner rod connects to the wedge to contract/expand the end effector, and the outer rod connects to the top nut to move the mechanism up and down.

"valves" outwards (Fig. 2C). The mechanism is made from 932 (SAE 660) bearing bronze and 440C stainless steel for low friction and saltwater compatibility. The neoprene boot protects the sliding elements from jamming with soil particles. The dimensions of the end effector are 9.9 cm (3.9 in) long (with end tip) and 1.52 cm (0.6 in) wide (when closed), expandable in width by 0.64 cm (0.25 in). These are on the same size scale as *E. directus*.

The substrate used in our experiments was 1mm diameter soda lime glass beads. This substrate was chosen because its density of 2.52 g/cm^3 is close to 2.66 g/cm^3 for real quartz sand [6], one of the substrates in which razor clams live [9]. The substrate was fully saturated with water in all tests and was contained in a 33 gal drum with the RoboClam mounted on top. Each test began with the end effector resting on the soil surface. Burrowing depth was judged from the soil surface and tests were only considered successful if the end effector penetrated greater than one body length. The only downward force applied to the end effector while burrowing was the weight of the up/down motion stage of the robot (2.5 kg); the lower piston did not apply any downwards force from pneumatic actuation and was only used for motion guidance and to retract the end effector at the end of each test.

Burrowing kinematics were controlled with a genetic algorithm (GA) [14], which approximates the evolution of a biological system by generating a population of parameters, in our case the in/out times and pressures, and then selecting the sets of parameters that yield the minimum 'cost', related to burrowing efficiency. Our intention was for the GA to optimize digging parameters for a minimum cost. This did not happen, but the GA provided a means of generating and then mixing random timescales and pressures within reasonable bounds, which yielded a variation in burrowing performance and GA cost.

The cost used in this work is the power law relationship, α, between burrowing energy expended by the robot (E) and downwards burrowing progress of the end effector (δ), where $E = \kappa\delta^{\alpha}$ and $\ln\kappa$ is the vertical intercept on the power law plot. Values of $\alpha \approx 1$ demonstrate burrowing via localized fluidization; values of $\alpha \approx 2$ indicate no fluidization and static soil. During each test, the end effector continued to run through in-out cycles until it stopped making vertical burrowing progress. The substrate was prepared and reset between tests by shaking it for 30 s using an industrial vibrator attached to the drum. Eighteen trials were run in this study, with each having an average of two generations of the GA and 10 tests per generation. In total, this work contains 362 individual burrowing tests.

RESULTS

Figure 3 shows the results from all burrowing tests included in this study. The data points are color coded corresponding to the GA cost function, with red indicating static soil and green indicating fluidized substrate. Black dots show tests that were either a failure or did not progress deeply enough to be considered successful. The data are plotted against the actual measured expansion and contraction times of the end effector.

The green dots in Fig. 3 are clustered around a contraction time of ≈ 0.075s (marked by the t_{min} line). These dots indicate that the RoboClam was able to successfully burrow using localized fluidization. All of the unsuccessful burrowing tests, as well as those in static soil, correspond to smaller contraction times than t_{min}.

DISCUSSION

Minimum Contraction Time to Induce Localized Fluidization

When *E. directus* or RoboClam's end effector contracts, it reduces its own volume. This change in volume must be compensated by pore fluid drawn into the region around the animal/mechanism. Movement of the pore fluid will cause drag on, and thus movement of, the particles within the localized zone of failed substrate around the animal. The Reynolds number of valve contraction fluid flow, calculated from *E. directus'* valve velocity, soil particle diameter, and the pore fluid density and viscosity, varies anywhere between 0.02 and 56, depending on particle size (0.002 to 2mm [8, 9, 6]), animal size (10 to 20cm)[2], and valve contraction velocity (v $\approx$ 0.011 to 0.028m/s [8]). As this range mostly falls within the regime of Stokes drag [15], the timescale for a soil particle to reach the valve velocity during contraction is

$$m_p \frac{dv_p}{dt} = 6\pi\mu d_p(v_v - v_p) \rightarrow t_{min} = \frac{d_p^2 \rho_p}{36\mu}, \quad (1)$$

where m_p is the mass of the particle, v_p is the particle velocity, d_p is the diameter of the particle, ρ_p is the density of the particle, v_v is the velocity of a contracting valve, μ is viscosity of the pore fluid, and t_{min} is the time constant of the differential equitation governing velocity change in Stokes flow.

This analysis yields $t_{min} = 0.075s$ for our substrate of 1mm soda lime glass beads in water. The center of the cluster of green dots in Fig. 3 corresponds with this time constant; all red and black dots correspond to smaller contraction times. This result indicates that end effector contraction times faster than t_{min} do not provide enough time for the substrate particles to advect with the pore fluid and reach a state of fluidization.

Maximum Contraction Time to Induce Localized Fluidization

If *E. directus* or RoboClam's end effector contracts too slowly, the soil will naturally collapse and landslide around the animal/machine without locally fluidizing. Figure 4 shows a soil element of arbitrary size h, l, w collapsing and beginning to slide at a failure angle θ_f. The strength of a soil is dictated by its friction angle φ; this angle is commonly seen as the slope angle in a pile of granular material, such as at a gravel yard. In a bed of soil, failure will occur along a slip plane at θ_f when an imbalance between horizontal and vertical stresses creates a resolved shear stress that exceeds the shear strength. The relationship between φ and θ_f is [6]

[2] from experimental observation

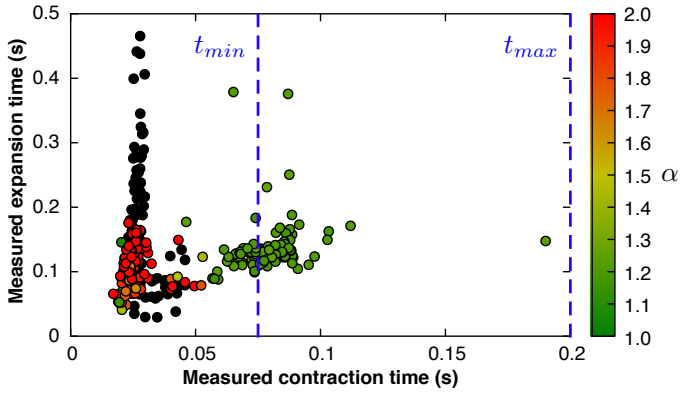

FIGURE 3. ROBOCLAM BURROWING PERFORMANCE. Plot shows the power law relationship α between energy and depth, where $E = \kappa\delta^{\alpha}$ and $\ln\kappa$ is the vertical intercept on the power law plot, for RoboClam burrowing in 1mm soda lime glass beads, dependent on contraction and expansion times of the end effector. Values of $\alpha \approx 1$ denote burrowing via localized fluidization; values of $\alpha \approx 2$ indicate no fluidization and static soil. Black dots are tests where burrowing depth was less than one body length and deemed unsuccessful. Timescales t_{min} and t_{max} show the calculated minimum and maximum contraction timescales to achieve fluidization with the end effector. Data constitute 362 tests during 18 trials.

$$\theta_f = \frac{\pi}{4} + \frac{\varphi}{2}. \quad (2)$$

The total stress in a submerged soil is composed of the effective stress between the particles themselves and the hydrostatic pressure of the pore fluid. Effective stresses in this paper are denoted with an apostrophe. Vertical effective stress in the soil, as a function of depth z, can be derived as

$$\sigma_v' = (1-\phi)(\rho_p - \rho_w)gz, \quad (3)$$

where ϕ is the void fraction in the soil (the fraction occupied by water), ρ_w is the density of water, and g is the gravitational constant. When the soil fails due to contraction of the end effector, the vertical effective stress at failure and equilibrium are equal because there is no change in soil depth ($\sigma_v' = \sigma_{vf}'$), but the horizontal effective is reduced. The relationship between horizontal and vertical effective stress at failure due to horizontal stress relaxation is characterized by the coefficient of active failure (K_a), which is dependent on the friction angle [6].

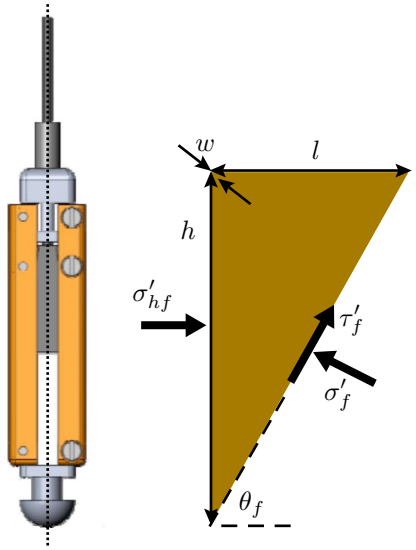

FIGURE 4. SOIL FAILURE DUE TO END EFFECTOR CONTRACTION. Dotted line denotes center line of the end effector. Triangle represents a soil wedge of arbitrary dimensions l , h, and w as it collapses and landslides towards the end effector at a failure angle θ_f. The horizontal effective stress in the soil at failure is σ'_{hf}; the resolved shear and normal stresses on the failure surface are τ'_f and σ'_f, respectively.

$$K_a = \frac{\sigma'_{hf}}{\sigma'_{vf}} = \frac{1-\sin\varphi}{1+\sin\varphi} \tag{4}$$

The horizontal acceleration on the triangular block (a_h) of soil in Fig. 4 can be found through conservation of momentum: $a_h = \frac{F_h}{m}$. The horizontal force acting on the block is found by combining Eqs. 3 and 4 and integrating over depth: $F_h = \int_0^h \sigma'_{hf} w dz$. The mass of the block is $\frac{1}{2}(\rho_p(1-\phi)+\rho_f\phi)lhw$. The characteristic time for the soil block to slide one characteristic length l is thus found by integrating the horizontal acceleration twice in terms of time.

$$t_{max} = \sqrt{\frac{2l}{a_h}} \tag{5}$$

It should be noted that all depth-dependent terms drop out of Eq. 5 and that l is simply a horizontal length scale.

The characteristic time calculated from Eq. 5 for 1mm soda lime glass beads saturated in water with h the same height as the end effector is t_{max} = 0.20s. This time is shown in Fig. 3, with all data points corresponding to smaller contraction timescales.

Maximum Expansion Time

E. directus and the RoboClam require enough time to move through the fluidized substrate and re-expand before it settles. The settling velocity of a suspension of particles in fluid is [16]

$$v_s = v_t \phi^n, \tag{6}$$

where v_t is the terminal velocity of a single particle in an infinite fluid and n is derived from the Archimedes number [17, 11]. The minimum void fraction to reach a fluidized state is called the incipient fluidization, ϕ_{fluid}, and is ≈ 0.41 for round particles [18]. As the particles settle, the void fraction will return to near its initial state, which for our substrate of 1mm soda lime glass beads was $\phi_0 = 0.38$. If the height of the fluidized region of particles is h_{fluid}, then the settled height is

$$h_{settle} = \frac{1-\phi_{fluid}}{1-\phi_0} h_{fluid}. \tag{7}$$

The settling time is found by combing Eqs. 6 and 7,

$$t_{settle} = \frac{h_{fluid} - h_{settle}}{v_s}. \tag{8}$$

Using 1mm soda lime glass beads and the end effector height in Eq. 8 yields t_{settle} = 2.2s. This time is well beyond the timescales plotted in Fig. 3, meaning the expansion time most likely had little effect on whether the RoboClam was able to achieve localized fluidization. This conclusion is supported by the vertical spread in the data with no correlation between fluidized and static/failed tests.

CONCLUSIONS

Localized fluidization burrowing offers a method of embedding rigid objects into underwater substrates with much less energy than is required to move through static soils. The fluidized region around the body is created by a quick contraction of volume – a purely kinematic effect. This method may be of value to many subsea applications where small, lightweight, compact burrowing systems are required.

This paper presents the critical timescales relevant to achieving localized fluidization. The timescales are derived from first principles and are experimentally validated through testing of the RoboClam burrowing robot. These timescales form the basis of design rules, which engineers can use to design burrowing systems of different size and design than the one presented in this

work, but that leverage the same borrowing method to achieve localized fluidization.

The work presented in this paper only relates to granular substrates. Future experimentation should investigate whether the theory also applies to cohesive substrates.

ACKNOWLEDGMENTS

This work was sponsored by the Battelle Memorial Institute, Bluefin Robotics, and the Chevron Corporation. The authors would like to thank Prof. Anette "Peko" Hosoi, Prof. Alex Slocum, and Dr. Robert Carnes for their contributions to this project.

REFERENCES

[1] Trueman, E., 1975. *The locomotion of soft-bodied animals*. Elsevier Science & Technology.

[2] Maladen, R., Ding, Y., Li, C., and Goldman, D., 2009. "Undulatory swimming in sand: Subsurface locomotion of the sandfish lizard". *Science,* ***325***(5938), p. 314.

[3] Dorgan, K., Jumars, P., Johnson, B., Boudreau, B., and Landis, E., 2005. "Burrowing mechanics: Burrow extension by crack propagation". *Nature,* ***433***(7025), p. 475.

[4] Wallace, H., 1968. "The dynamics of nematode movement". *Annual Review of Phytopathology,* ***6***(1), pp. 91–114.

[5] Jung, S., 2010. "Caenorhabditis elegans swimming in a saturated particulate system". *Physics of Fluids,* ***22***, p. 031903.

[6] Terzaghi, K., Peck, R., and Mesri, G., 1996. *Soil mechanics in engineering practice*. Wiley-Interscience.

[7] Robertson, P., and Campanella, R., 1983. "Interpretation of cone penetration tests. Part I: Sand". *Canadian Geotechnical Journal,* ***20***(4), pp. 718–733.

[8] Trueman, E., 1967. "The dynamics of burrowing in Ensis (Bivalvia)". *Proceedings of the Royal Society of London. Series B. Biological Sciences,* ***166***(1005), p. 459.

[9] Holland, A., and Dean, J., 1977. "The biology of the stout razor clamTagelus plebeius: I. Animal-sediment relationships, feeding mechanism, and community biology". *Chesapeake Science,* ***18***(1), pp. 58–66.

[10] Energizer Battery Company, 2009. Energizer E91 AA Battery Product Datasheet. `http://data.energizer.com/PDFs/E91.pdf`.

[11] Winter, V, A., Deits, R., and Hosoi, A., 2012. "Localized Fluidization Burrowing Mechanics of Ensis directus". *The Journal of Experimental Biology,* ***215***(12), pp. 2072–2080.

[12] Winter, V, A., and Hosoi, A., 2011. "Identification and Evaluation of the Atlantic Razor Clam (*Ensis directus*) for biologically inspired subsea burrowing systems". *Integrative and Comparative Biology,* ***51***(1), pp. 151–157.

[13] Winter, V, A., Deits, R., Dorsch, D., and Hosoi, A.E., S. A., 2010. "Teaching RoboClam to Dig: The Design, Testing, and Genetic Algorithm Optimization of a Biomimetic Robot". In Proceedings of the IEEE/RSJ 2010 International Conference on Intelligent Robots and Systems (IROS), no. WeET11.3.

[14] Haupt, R., and Haupt, S., 2004. *Practical genetic algorithms*. Wiley-Interscience.

[15] Kundu, P., and Cohen, I., 2004. *Fluid Mechanics*. Elsevier Academic Press.

[16] Richardson, J., and Zaki, W., 1954. "Sedimentation and fluidisation: Part I". *Chemical Engineering Research and Design,* ***32***(a), pp. 35–53.

[17] Khan, A., and Richardson, J., 1989. "Fluid-particle interactions and flow characteristics of fluidized beds and settling suspensions of spherical particles". *Chemical Engineering Communications,* ***78***(1), pp. 111–130.

[18] Wen, C., and Yu, Y., 1966. "Mechanics of fluidization". In Chem. Eng. Prog. Symp. Ser, Vol. 62, pp. 100–111.